International Journal of Sediment Research 37 (2022) 214–228

Contents lists available at ScienceDirect

International Journal of Sediment Research

journal homepage: www.elsevier.com/locate/ijsrc

Original Research

Impacts of dams and land-use changes on hydromorphology of braided channels in the Lhasa River of the Qinghai-Tibet Plateau, China

Yuchi You [a], Zhiwei Li [a, b], Peng Gao [c, *], Tiesong Hu [b]

[a] School of Hydraulic Engineering, Changsha University of Science & Technology, Changsha, 410114, China
[b] State Key Laboratory of Water Resources and Hydropower Engineering Science, Wuhan University, Wuhan, 430072, China
[c] Department of Geography and the Environment, Syracuse University, Syracuse, NY, 13244, USA

ARTICLE INFO

Article history:
Received 13 November 2020
Received in revised form
2 July 2021
Accepted 12 July 2021
Available online 31 July 2021

Keywords:
Braided river
Channel morphology
Human activities
Dam impact

ABSTRACT

Among braided rivers developed on the Qinghai-Tibet Plateau of China at very high elevations (>3,500 m), the middle and lower reaches of the Lhasa River have been affected by comprehensive human activities mainly involving dam construction, urbanization, farming, afforestation, and mining. In the current study, the impacts of these human activities on hydrology and morphology of the four braided reaches downstream of a cascaded of two dams are investigated. The study period was divided into 1985–2006 (P1), 2006–2013 (P2), and 2013–2019 (P3), representing the natural and changed flow regimes by dams. Using available daily discharge data at two stations within the four braided reaches, dam-induced hydrological alteration was analyzed based on the indicators of hydrologic alteration and range of variability approach and key discharge proxies were calculated. Remotely sensed images also were selected in the three periods and morphological metrics extracted from them were compared for the four reaches among these periods. Attenuated hydrological regimes were found for only two reaches. The total channel width (W_c) and braiding intensity (BI_t) followed different temporal trends among the four reaches. Annual average shift rates of the main channel in the four reaches were higher in the short (P2–P3) than in the long (P1–P2 and P1–P3) periods. The longitudinal changes of W_c and the number of channels did not have any identifiable trend among the four reaches. By linking the morphological changes to quantified spatial and temporal patterns of various human activities, it was found that (1) the two dams had insignificant impact on channel morphology, suggesting that the studied braided river might have a short relaxation time and (2) the evolutional trajectories of morphological changes in most of the four reaches were similar, suggesting that temporal trends of morphological changes due to complex human activities are not affected by the different physiographic settings of the reaches. Continuous exploitation of the valley area requires comprehensive river management strategies for coordinating various human activities.

1. Introduction

Braided rivers exist in various alluvial environments, such as mountainous regions and lower-gradient alluvial plains (Ashmore, 2013; Downs & Piégay, 2019; Limaye, 2017; Stecca et al., 2019). These multithread channels with relatively shallow flows and their ambient floodplains jointly form a complex riverine wetland, where braided rivers are turned into dynamic habitats for aquatic, terrestrial, and bird species by pulsed floods (Belletti et al., 2012; Bertoldi, Gurnell, et al., 2009; Boruah et al., 2008; Paetzold et al., 2005; Piégay et al., 2009), and become vital riverine ecosystems (Gran et al., 2015; Ligon et al., 1995; Nilsson et al., 1997; Shields & Milhous, 1992; Zhang et al., 2011).

Braided channels alternately diverge and converge, coupled with lateral erosion under the condition of (near) bankfull flows during flood seasons (Ashmore et al., 2011; Bertoldi, Zanoni, & Tubino, 2009). Most previous studies have concentrated on morphodynamic processes of braided rivers located in low-altitude alluvial plains that may be exemplified by the Jamuna-Brahmaputra River, lower Yellow River, and estuary zones (Dubey et al., 2014; Li et al., 2017, 2018; Lotsari et al., 2014; Schuurman et al., 2013), and relatively medium-altitude valleys, such as the

* Corresponding author.
E-mail address: pegao@syr.edu (P. Gao).

https://doi.org/10.1016/j.ijsrc.2021.07.003

Piave and Waitaki rivers (Stecca et al., 2019; Ziliani et al., 2020). The braided reaches of the Lhasa River, however, are located in the southeast Qinghai-Tibet Plateau (QTP) with an average elevation of above 3,650 m. Similar to others in the QTP that are distributed in the source regions of the Yellow, Yangtze, Lancang, and Yarlung Tsangpo river basins (Li et al, 2016, 2020a, b; Wang et al., 2016), these braided reaches play vital ecological roles in maintaining local riverine ecosystems. Nonetheless, the braided channels of the Lhasa River have been uniquely subject to a variety of increasingly complex and intense human activities in the past three decades (Yang & Hu, 2013). Hitherto, it is still unknown how their hydrology and morphology have responded the intense human disturbance. The current study aims at revealing these responses.

Sitting in the cold and arid Lhasa River valley, the braided reaches serve as vital river corridors in sustaining the local eco-hydrological balance and living environments of about 0.7 million residents in the Lhasa River basin (Jiang et al., 2019; Li & Xu, 2015; Wu et al., 2018; Zhang et al., 2010). In particular, the braided reaches are the main sources of drinking water for Lhasa and nearby towns, as well as for agricultural irrigation and industrial usage. Owing to the severe shortage of electric power in the Lhasa City before 2000, Zhikong and Pangduo dams were successively built on the main channel of the upper Lhasa River basin in 2006 and 2013, respectively, which directly altered the natural regimes of runoff and sediment flux (Yang & Hu, 2013). Moreover, rapid population growth and socioeconomic development of Lhasa in the last three decades has catalyzed (1) continuous land expansion of the city and smaller towns along the river, (2) agricultural development within the wider sections of the valley, (3) in-channel hydraulic projects, and (4) afforestation for controlling aeolian erosion processes (Chen et al., 2019; Tao et al., 2019). These human activities have profoundly disturbed the natural evolutional trajectory of the braided channels both directly and indirectly, making them the most intensely interrupted and fragile river systems across the QTP.

Morphological responses of braided rivers to human interruption has been the subject of many previous studies. For example, the operation of a cascade of reservoirs resulted in reduction of braided channel activity (Chien, 1985; Stecca et al., 2019; Wang et al., 2007; Wu et al., 2018), and bank protection or embankment construction restrained free scouring of and sedimentation in braided channels (Li et al., 2017; Stecca et al., 2019). A long-standing challenge is that these responses are time sensitive, and, thus, the required time for reaching a new equilibrium varies depending on types of disturbance (Han et al., 2020; Nelson et al., 2013; Richard et al., 2005; Xia et al., 2014). Estimating the morphological response of braided rivers is further confounded by possibly altered hydrological regimes due to increased glacial runoff and extreme flood events in the context of global climate change (Bakker et al., 2019; Chalise et al., 2021; Ziliani et al., 2020). Consequently, morphological changes of the braided channels in the Lhasa River in response to intense anthropogenic activities cannot be simply inferred from findings in braided rivers located in other regions as the impacts of human activities on rivers often are site-specific (Csiki & Rhoads, 2014). There is a clear knowledge gap regarding the human impact on the Lhasa River. The objective of the current study is to reveal the morphological response of the Lhasa River to comprehensive human activities over a period of three decades. Scientifically, the current study will yield useful results to facilitate the derivation of general rules of river adjustment under the influence of anthropogenic activities at the global scale (Downs & Piégay, 2019) because knowledge of river adjustment is lacking in this area with unique physiographic characteristics. Practically, the current study will help local government strategically manage human interventions on the Lhasa River, which is a vital habitat supporting the city of Lhasa, which is the center of Tibetan politics, economics, culture, and religion.

The objectives of the current study by focusing on the downstream braided reach of the Lhasa River below the two dams are (1) examining the hydrological responses to the two constructed dams; and (2) revealing morphological responses of the studied river reach to other human activities. Using available daily discharge data over the past three decades at the two gauging stations within the studied reach, the altered hydrological characteristics are examined. High-resolution images also are obtained from Google Earth and Gaofen (http://www.cresda.com/CN/index.shtml) to quantify the scope and changes of human activities in the valley of the studied reach. By selecting three sets of Landsat images in three representative years in the period 1985–2019, three morphological indices are computed, the total channel width, braiding intensity, and lateral shift rate of the main channel, and their spatiotemporal changes are examined in the four sub-reaches that comprise the studied braided reach. Finally, the connection between historical changes of various human activities and morphological adjustment of these sub-reaches is revealed, and the river management implications are examined.

2. Materials and methods

2.1. The study area

Lhasa River is the largest tributary of the Yarlung Tsangpo River in the southern QTP (see the inset in Fig. 1a). The middle and lower Lhasa River develops one of the highest braided channels on the earth with an elevation of 3,590–4,030 m.a.s.l. It ranges from 29°20′–31°15′ N, 90°05′–93°20′ E, with a total length of 568 km and a basin area of 32,896 km^2 (Fig. 1a). The Lhasa River basin is dominated by a semi-arid climate, characterized by strong solar radiation, long sunshine hours, low air temperature, and large differences of diurnal temperature. It only experiences two seasons annually, the wet and dry seasons. The former is short and warm, typically from June to September, while the latter is long and cold, usually extending from October to May. The mean annual precipitation ranges between 340 and 700 mm, 90% of which is concentrated in the wet season. The mean annual evaporation is in the range between 660 and 1,268 mm.

The selected study reach stretches about 145.7 km in the valley of the middle and lower Lhasa River basin from Zhikong Dam to the confluence with the Yarlung Tsangpo River at Qushui, and is joined by three tributaries, the Mozhumaqu, Pengboqu, and Duilongqu rivers (Fig. 1a and 1b). The valley is filled with alluvial and fluvial deposits with a mean gradient of 0.2%. The entire valley floor serves as the river corridor. Pangduo (upstream) and Zhikong (downstream) dams (Fig. 1a) were constructed in the upstream section of the study reach in 2013 and 2006, respectively. Pangduo Dam controls a watershed area of 16,370 km^2 with a mean annual runoff of 6.21×10^9 m^3 and a total storage capacity of 1.23×10^9 m^3. Its reservoir serves as a comprehensive hydropower project of water conservancy and its utilization has multifunctional services including irrigation, power generation, flood control, and freshwater supply. Zhikong Dam is located 65 km downstream from Pangduo Dam, and is 106 km upstream of Lhasa (Fig. 1a and 1b). It controls a drainage area of 20,179 km^2 with a mean annual runoff of 7.47×10^9 m^3 and a total storage capacity of 0.224×10^9 m^3. The primary function of the Zhikong Reservoir is generation of hydroelectric power, accompanied by side functions for irrigation and flood control. The total annual runoff volume of the studied reach is 9.08×10^9 m^3 with a mean annual discharge of 242 and 287 m^3/s at the two gauging (i.e., Tangjia and Lhasa) stations (Fig. 1b). Their average runoff coefficients are 0.78 and 0.75, respectively.

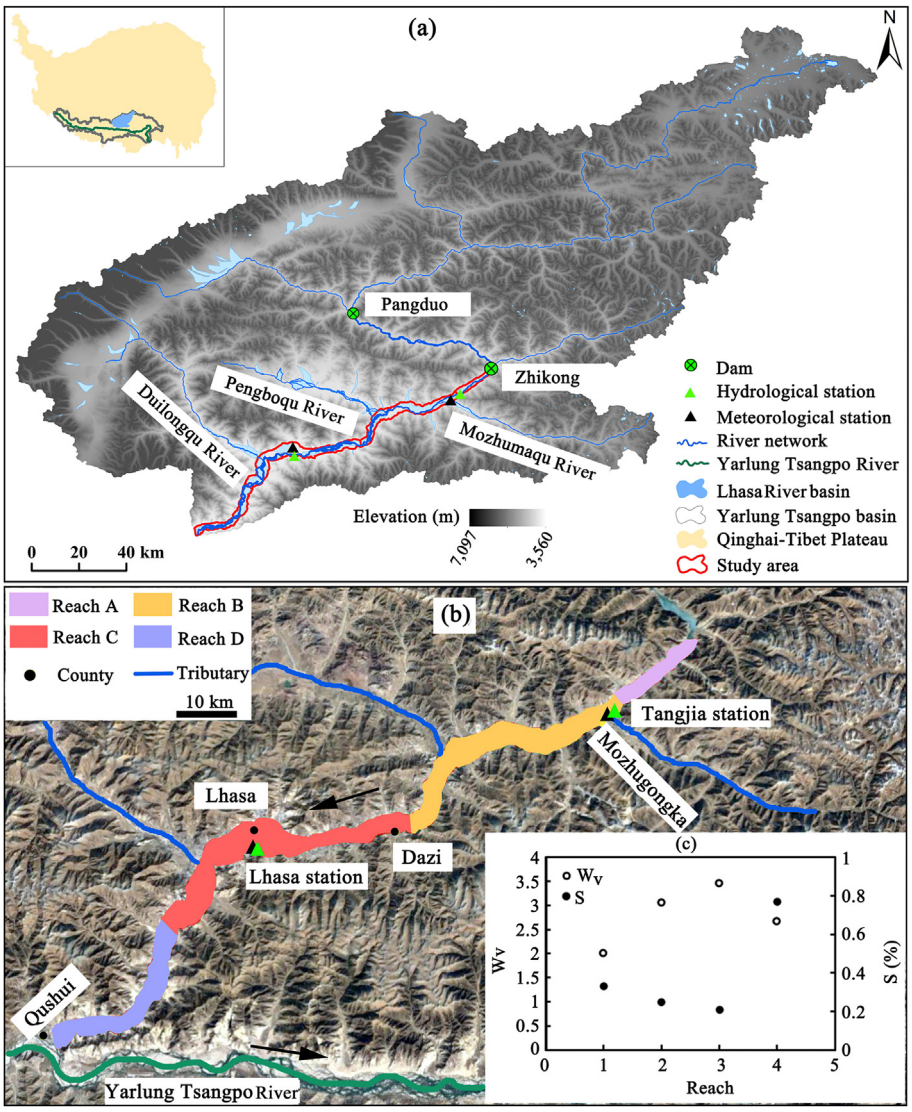

Fig. 1. Geography and geomorphologic settings of the study area. (a) Geographic locations of the studied braided reach, meteorological and hydrological stations, and the two upstream dams; (b) the four (A, B, C, and D) smaller reaches within the study reach and their geographic relationships with the two hydrological stations and three tributaries; (c) variations of the geomorphological characteristics among the four small reaches (reaches A, B, C, and D are represented by 1, 2, 3, and 4, respectively, on the horizontal axis).

The study reach was divided into four smaller reaches, which are A, B, C, and D from upstream to downstream (Fig. 1b). Reach A is immediately below Zhikong Dam. It extends for about 16 km with a mean gradient of 0.33% and its valley covers the area of 33.36 km^2. No tributary flows into this reach. Reach B is about 46.3 km long with a mean gradient of 0.25% and has a valley area of 141.16 km^2. Reach C is 49.8 km long with a mean valley slope of 0.21%. It has a valley area of 172.28 km^2. Reach D is 31 km long with a mean gradient of 0.77% and covers the area of 82.92 km^2. These four reaches have different mean gradients S and mean valley widths W_v (Fig. 1c), representing spatially variable channel morphology and valley settings of the study reach. The current study focused on the temporal responses of hydrology and channel morphology to the dynamic human activities from 1985 to 2019. To correctly reflect the impact of the two dams constructed at different time on hydrology and channel morphology, the study period was divided into three periods, 1985–2006 (P1), 2006–2013 (P2), and 2013–2019 (P3), representing the natural flow regime, the changed flow regime due to the completion of Zhikong Dam (Fig. 1a), and the further altered flow regime caused by the completion of Pangduo Dam (Fig. 1a), respectively.

2.2. Methods

2.2.1. Data acquisition and error assessment

Daily discharges from 1956 to 2016 were obtained from the Tangjia and Lhasa hydrological stations for characterizing the hydrological regime and its temporal changes in the study reach (data are missing from 1956 to 1962 and in 1996 for the Tangjia station, while those from 1969 to 1972 are missing for the Lhasa station). Landsat images ranging between 1990 and 2018 and Gaofen (GF) (http://www.cresda.com/CN/index.shtml) images in 2015 covering different parts of the study reach were initially selected. These images have been pre-processed for radiative correction and georeferencing (http://www.gscloud.cn). Although most of the images were obtained in the dry season when water discharges are generally low, there are still two caveats. First, some only cover a proportion of the study reach. Second, some were obtained in years when daily discharges are not available, such that it is uncertain whether channel morphology extracted from them may be comparable with that from other images. Therefore, two sub-sets of the original images are carefully selected (Table 1). The first set includes Landsat images in 1990, 2010, and 2015/2016. These images cover

all four reaches and represent the three time periods, P1, P2, and P3. In a given year, images covering different reaches may not be always from the same dates. The second set contains Landsat images only available in February, April, October, and December of 2016 to reflect the intra-annual changes of channel morphology.

For the first set of images, the associated daily discharges were not exactly the same (Table 1). To test whether these discharge variations would affect the extracted channel morphology, and, thus, hinder the comparison among the four reaches, two types of error analysis were applied. In the first one, we used the Landsat and GF images in 2015 that are partially overlapped in reaches A, B (sub-area B1 and B2), and C (sub-area C1 and C2) (Table 2) to calculate the total channel width for the selected transects and compared them. The result (reaches A, B1, B2, C1, and C2) showed (Fig. 2a) that the average difference between the two was 9.36 m. Given that the GF2 images have the resolution of 4–8 m, this difference suggests that extracting channel widths from the Landsat data would lead to the error of 9.36 m, which is much less than the Landsat resolution 30 m. It appears that the error possibly arising during morphological extraction from the Landsat images is limited. However, the images used for comparison are associated with different daily discharges (Table 2). It is still not sure how differences in discharges among the Landsat images used for comparison would affect the morphological comparison. In the second test, the calculated widths were compared for two sets of images in February 16 and 23 and April 27, 2016 when the discharges for the four reaches were different (Table 1). The comparison showed (Fig. 2b) that the average difference could be 33.7 m, slightly greater than the resolution (30 m). Given that the discharge differences for reaches A, B, C, and D among P1, P2, and P3 were all within the range of discharges among the tested images, the impact of different discharges among the selected Landsat images on extracted channel morphology is a constraint.

A variety of human activities can be identified in these four reaches. They may be generally classified into four types: (1) Agricultural activity, which is represented by farmland; (2) construction activity, which mainly includes urbanization, and construction of roads, bridges, small canals, and check dams, is represented by the area of urban lands and identifiable construction sites henceforth referred to as urban area; (3) afforestation, which refers to trees planted by human beings on sand/gravel bars and valley floors within and outside of the braided system, and is represented by their coverage (planting) areas; and (4) mining,

Table 2
Two sets of remotely sensed images with different resolutions for error assessment.

Image type	Date	Daily discharge (m^3/s)	Covered reach
GF1	12/12/2015	45.5	A, B
GF2	12/29/2015	94.1	B
	12/29/2015	70.3	C
Landsat 8	12/30/2015	78.7	A, B
	12/30/2015	68.7	C

which denotes the areas disturbed by sandpits and is represented by the disturbed area. Areas of construction, farmland, and mining were extracted from the three Google Earth images (with the resolution of about 1 m) from 1990, 2010, and 2019, which represent periods P1, P2, and P3, respectively. Areas of afforestation (i.e., planting trees) also were determined from the three selected sets of Landsat images (Fig. 3a–3d). Their spatial and temporal variations among the four smaller reaches then were examined.

2.2.2. Hydrologic analysis

The obtained daily discharge data were used to determine the Indicators of Hydrologic Alteration and Range of Variability Approach (IHA-RVA) (Richter et al., 1998) for quantifying the degree of the variability in the natural hydrologic regime of the study river (i.e., the Lhasa River) due to construction and operation of the cascade of two reservoirs. The IHA-RVA generally involves 32 hydrologic metrics (Magilligan & Nislow, 2005; Song et al., 2020; Yu et al., 2016) to identify alteration that occurred in the five critical components of the natural flow regime, i.e., magnitude, frequency, duration, timing, and rate of change (Poff et al., 1997; Richter et al., 1996). This method has been widely used to reveal the impact of dams on hydrological processes of many rivers in the world (Gao et al., 2012; Gierszewski et al., 2020; Jiang et al., 2019; Li et al., 2017; Remo et al., 2018; Sojka et al., 2016; Song et al., 2020).

Alteration of the hydrological regime possibly caused by the cascade of the two dams was examined using the IHA-RVA for determining changes of the indicators between the periods P1–P2, P1–P3, and P2–P3. Because many of the 32 indicators in IHA-RVA are intercorrelated, using all of them would lead to considerable information redundancy (Gao et al., 2009). Yet, no general rule is available to guide the section of an appropriate sub-group from the 32 indicators. Given that the current study focuses on morphological responses of the braided reaches to hydrological alteration,

Table 1
Two selected sets of remotely sensed images.

	Image type	Date	Daily discharge (m^3/s)	Covered reach	Period
Set 1	Landsat 5	03/03/1990	60.4 (LS*)	D	P1
		04/13/1990	43.0 (TJ**)	A, B	
		04/13/1990	55.2 (LS)	C	
	Landsat 8	04/11/2010	48.5 (LS)	C, D	P2
		05/22/2010	40.8 (TJ)	A, B	
	Landsat 8	12/21/2015	60.4 (LS)	D	P3
		02/16/2016	50.8 (TJ)	A, B	
		02/23/2016	19.6 (LS)	C	
Set 2	Landsat 8	02/16/2016	50.8 (TJ)	A, B	P3
		02/23/2016	19.6 (LS)	C, D	
		04/04/2016	66.7 (TJ)	A	
		04/27/2016	77.6 (TJ)	B	
		04/27/2016	50.8 (LS)	C, D	
		10/20/2016	515 (TJ)	B	
		10/20/2016	461 (LS)	C, D	
		10/29/2016	144 (TJ)	A	
		12/07/2016	67.0 (TJ)	B	
		12/07/2016	76.8 (LS)	C, D	
		12/16/2016	50.5 (TJ)	A	

Note: *LS - the Lhasa hydrological station, **TJ - the Tangjia hydrological station.

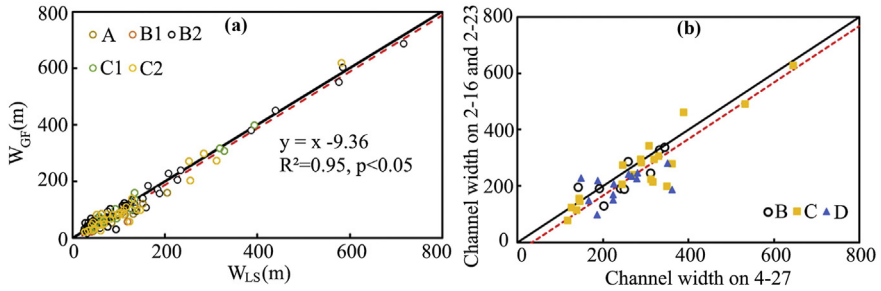

Fig. 2. Assessment of errors possibly rising from morphology extraction from remotely sensed images. (a) Comparison of the total channel widths obtained from the Landsat images (W_{LS}) with those from the Gaofen images (W_{GF}) in reaches A, B (sub-area B1 and B2) and C (sub-area C1 and C2); and (b) comparison of W_{LS} values extracted from the images obtained on 4/27/2016 with those on 2/16/2016 and 2/23/2016. The dotted lines are the linear fitting results of the data.

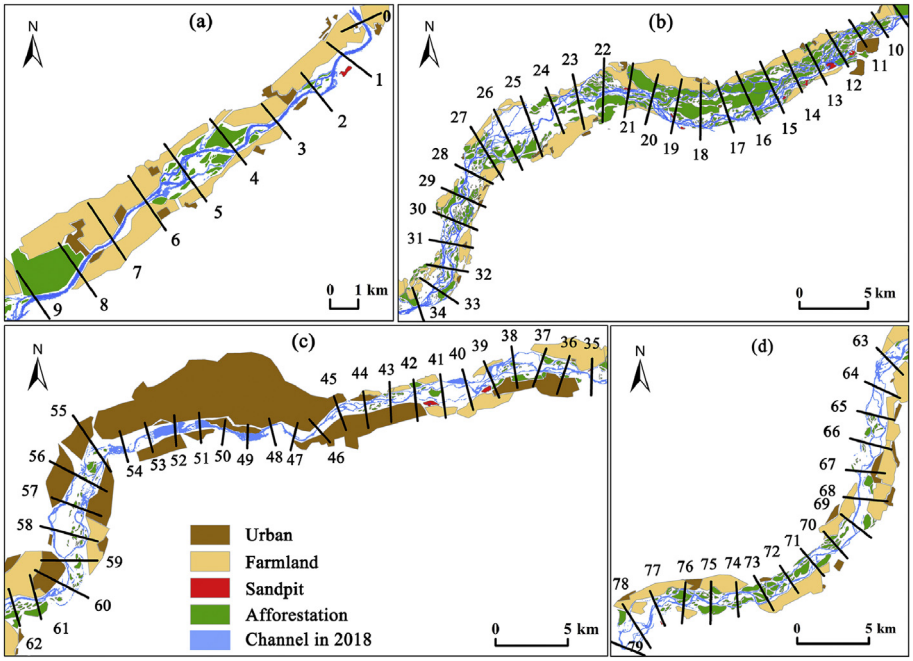

Fig. 3. Percentages of the areas occupied by the three main types of human activities in the four reaches (a, b, c, and d), construction, farmland, and afforestation (areas occupied by sandpits are too small to be included here). Although areas of afforestation were obtained in one year (2019), while those of other types were obtained in a different year (2016), these results were combined to represent current land-use types.

Han et al. (2020) was followed and selected 22 of the most relevant indicators were selected. They are 12 monthly mean discharges and 10 extreme (maximum and minimum) discharges for 1-, 3-, 7-, 30-, and 90-days. For each selected indicator, the mean and coefficient of variation (CV) were calculated. Their degree of change is quantified using the normalized function (Ma et al., 2014):

$$d_k = \frac{1 - \exp(-av_k)}{1 + \exp(-av_k)} \quad (1)$$

where d_k is the alteration degree of the k-th indicator, $a = 3$, and v_k is the deviation ratio for each period of change:

$$v_k = \frac{P_{kA} - P_{kB}}{P_{kB}} \quad (2)$$

where P_{kA} and P_{kB} are the values of the k-th indicator for each period of changes. The value of d_k ranges between −1 and 1 with negative and positive values indicating a decrease and an increase of the indicator, respectively. The magnitude of d_k (i.e., $|d_k|$) may be divided into three categories, $|d_k| < 0.33$ for minor alteration, $0.33 \leq |d_k| < 0.67$ for a moderate alteration, and $|d_k| \geq 0.67$ for a high alteration (Ma et al., 2014; Richter et al., 1998). Values of $|d_k|$ for all 22 selected indicators were subsequently used to determine the overall degree of hydrological alteration (D_T) for the three periods:

$$D_T = \frac{1}{18}\sum_{k=1}^{18} |d_k| \quad (3)$$

These 22 indicators and D_T values were calculated only for the Tangjia gauging station as flows at this location have not been affected by the three tributaries flowing into the lower portion of the study reach (Fig. 1b). Furthermore, flood frequency analysis was applied for determining discharges with recurrence intervals of one, two, and five years (i.e., Q_1, Q_2, and Q_5, respectively) for both stations. Using these discharges, average days of a year with $Q > Q_1$, Q_2, and Q_5, respectively, were determined. Because this value for Q_2 and Q_5 is too small, only the average number days for Q_1 is reported. Based on these calculations, hydrological properties were compared between the two stations for P1, P2, and P3.

2.2.3. Morphological analysis

The Normalized Difference Vegetation Index (NDVI) and Modified Normalized Difference Water Index (MNDWI) are two commonly used indices for distinguishing water bodies from land surfaces in remotely sensed images (Ju & Masek, 2016; Ozyavuz et al., 2015; Xu, 2006; Zhou et al., 2015). After testing both indices in the study reach, it was found that NDVI is better in the current case for identifying boundaries of braided channels, and, thus, NDVI was used to extract braided channels from each selected Landsat image (Table 1). Moreover, NDVI values in Landsat images were used to determine vegetated areas in 2010 and 2019 (i.e., P2 and P3). The threshold value of NDVI for identifying vegetation was determined by comparing the vegetation area identified from the 2019 Landsat image with that from the 2019 Google Earth image.

To examine both reach-averaged and longitudinal variations of channel morphology, three types of morphological metrics were calculated based on 80 transects pre-selected along the four reaches (Fig. 3a–3d). The first is the total channel width along each transect (W_c), defined as the sum of widths for all identified channels along a given transect. This definition is different from the commonly used active channel width, which is the reach-averaged width of both channels and non-vegetated bars (Ziliani & Surian, 2012). W_c was used because (1) more and more valley areas in the four reaches have been occupied by farming and urban areas since 1990, such that the change of the active channel width would not solely reflect the impact of upstream dams; and (2) it also has been used in previous studies for addressing the downstream impact of dams on channel morphology (Sanchis-Ibor et al., 2019; Surian & Rinaldi, 2003).

The second metric is braiding intensity (BI_t) for each reach:

$$BI_t = \sum_{i=1}^{n} \frac{N_{ci}}{n} \tag{4}$$

where N_{ci} is the number of the braided channels along the i-th transect and n is the number of the selected transects in each reach. The third metric is the lateral shifting rate of the main braided channel (R_l) which is calculated in two steps. In the first step, the two centerlines of the main channels for the 1990–2010, 2010–2019, and 1990–2019 periods were overlaid and areas of changes were identified and calculated. This area was treated as an error if it was too thin (i.e., the average displacement is at least 10 times less than the length of the overlaid channel segment) or the area is less than 100 m^2. In the second step, the identified areas were divided by the length of the channel segment in the earlier period to get the lateral displacement. The R_l value was then determined by dividing this displacement by the number of years in a given period.

The obtained values of W_c, BI_t, and R_l were subsequently compared (1) at the reach scale among the four selected reaches (i.e., A, B, C, and D) and (2) along the selected transects in the longitudinal direction. In addition, these values were examined among months in 2016 to illustrate the intra-annual characteristics of channel morphology.

3. Results

3.1. Spatially and temporally variable human activities

3.1.1. Current spatial patterns

The four types of human activities in 2019 demonstrate various spatial variations in the four reaches (Table 3 and Fig. 3a and 3d). In reach A that was divided into 10 transects (i.e., T0–T9), about 47% of the valley area is farmland, largely occupying the floodplains of the sinuous segments in the current braided channels. The second largest area, which takes about 14% of the valley area, is covered by afforestation areas. The artificially planted trees are on sand and gravel bars distributed among the braided segments in the upper and middle sections of the reach and the floodplain of the downstream meandering segment. In addition, there are about 1.66 km^2 of the valley area occupied by small villages and towns, accounting for about 5% of the total area. One mining site sandpit has disturbed the area of 0.06 km^2 (Fig. 3a), only taking less than 0.18% of the total valley area. The human disturbed area occupies about 66.5% of the valley area in reach A with farming as the dominant type of human activities (Table 3).

In reach B that includes 25 transects from T10 to T34 (Fig. 3b), the dominant types of human activities are afforestation and farming, comprising about 27% and 20% of the total valley area, respectively (Table 3). Afforestation leads to artificially planted trees distributed on sand/gravel bars and edges of the farmland throughout the reach and farming results in agricultural lands flanking both sides of the river system. Urban areas in this reach primarily focus on the upstream valley, serving as a small town (i.e., Mozhugongka) and very limited areas are disturbed by mining, indicating their localized effect on neighboring channel segments (Fig. 3b). About 50.8% of the total area is affected by human activities, which is less than that in reach A (Table 3).

In reach C that includes 28 transects from T35 to T62 (Fig. 3c), 64% of its valley area is disturbed by various human activities (Table 3). The dominant human activity comprises urban areas, accounting for about 55% of the total valley area. Continuous urbanization is the main factor (Fig. 3c), which is mainly from the result of the expansion of Lhasa, located in the middle of the reach and further extended to a proportion of the reach in the upstream and downstream directions. Although the three check dams in the middle of the reach could not be included into the urban area, they have significant impact on channel morphology and cannot be ignored. Farmland only accounts for about 13.5% of the total area, much less than in reaches A and B. Farmland primarily is distributed on the valley sides in both upstream and downstream portions of the reach. This is because a proportion of farmland has been converted into urban lands. For example, from 2006 to 2011, about 24.48 km^2 of farmland neighboring the Lhasa were transformed into urban lands. Only 3.4% of the valley area was artificially planted (Table 3). These trees spread over the majority of the bars in the upstream and downstream braidplains, apparently stabilizing these bars. Mining sites again have disturbed a very confined area in the upstream section, which only comprises 0.26% of the total area. Thus, sandpit influence on channels is limited.

In reach D that is divided into 27 transects from T63 to T79 (Fig. 3d), the dominant human activity is farming, whose lands comprise about 31.5% of the total valley area (Table 3). They are larger than those in reaches B and C, but less than those in reach A. These lands are distributed across the entire reach on either side of the valley. Afforestation is the second largest type of human activity affecting bars mainly in the middle and downstream sections of the reach (Fig. 3d). These areas comprise about 10.5% of the total valley area, less than in reaches A and B (Table 3). The urban areas only comprise about 5% of the total which is comparable to that in reaches A and B. Urban areas spread further away from the channels, neighboring the outside edges of the farmland. Mining

Table 3
Areas (%) of the four types of human activities in the four reaches.

Reach	Farmland	Afforestation	Urban	Sandpit
A	46.99	14.33	4.96	0.18
B	20.35	27.34	2.60	0.47
C	13.45	3.38	55.17	0.26
D	31.46	10.53	4.92	0.02

apparently has negligible impact on the channels because of its very small disturbed area, only comprising about 0.02% of the total (Table 3).

3.1.2. Temporal changes

Among the four reaches, the percent of urban area in 1990 was the highest in reach C, which was about 10.1%, while it was less than 0.2% in the other reaches (Fig. 4a). From 1990 to 2010, this percentage increased to about 26% in reach C, but only increased marginally in other three reaches. In 2019, construction accounted for about 55% of the total area in reach C, but still had limited increases in the other reaches, accounting for about 5.0%, 2.6%, and 4.9% in reaches A, B, and D, respectively. The significant increase of this area from 1990 to 2019 in reach C signifies the expansion of Lhasa, and is consistent with the continuous increase of population in this city from 267,000 in 1990 to 484,000 in 2010 and 554,000 in 2018.

The farmland in 1990 was the highest in reach A, comprising about 58.5% of the total area, followed by 20.8%, 29.4%, and 31.3% in reaches B, C, and D, respectively (Fig. 4b). This percentage decreased continuously from 1990 to 2019 in reaches A and C, which were 47% and 13.4% in 2019, respectively. It increased slightly from 1990 to 2010 in reach B, which was 23.6%, and then decreased again to 20.4% in 2019. In reach D, the percentage roughly remained similar at about 31% over the entire study period. Apparently, the decrease of farmland from P1 to P3 was accompanied by the simultaneous increase of the urban area in reaches A and C, suggesting that the former might be replaced by the latter.

In 1990 when the afforestation was not implemented, the area of vegetation was impossible to identify from the Google Earth images. Thus, though they are unknown, these areas in all four reaches should be very small. In 2010, the percentage of this area was detectable and were 0.5%, 5.6%, 3.9%, and 4.8% for reaches A, B, C, and D, respectively (Fig. 4c). Since then, afforestation has been accelerated, reaching 14.3%, 27.3%, 3.4%, and 10.5% in 2019 for the four reaches, respectively (Fig. 4c). The significant increase in the area with planted trees from P2 to P3 occurred in reaches A and B, though reach D also experienced an increase of this area. However, reach C showed a minor decrease of this area during this period, possibly because expansion of Lhasa dominated the intensified human activities in this reach. Mining is generally much less intensive than other types of human activities (Table 3). Its development reflects the need for urbanization and other construction, which was accelerated from 2010 to 2019. Thus, sandpits mainly occurred in the P2–P3 period.

3.2. Changes of hydrological regimes

3.2.1. Reaches A and B

Between periods P1 and P2, both mean monthly and extreme discharges were reduced in magnitude, many of which had moderate degrees of reduction (see the blue bars in Fig. 5a and 5b). Variations of mean monthly discharges for summer months, whose discharges are generally high, decreased with moderate to high degrees, whereas those in other months, whose discharges are generally low, increased with high degrees (Fig. 5c). For the extreme discharges, however, their values were all reduced, though the degree of reduction was mostly minor except the one for December (Fig. 5a). These trends indicate that the closure of the first (i.e., Zhikong) dam, which is closer to the study reach than the second dam, reduced the magnitudes of river flows and variations of high flows during summer, but increased the variations of low flows during winter and spring.

Between periods P1 and P3, mean monthly discharges decreased from April to December except for July with a moderate degree of change in summer months, but increased in winter months and July with moderate and high degrees of changes (i.e., the red bars in Fig. 5a). Changes of the extreme discharges followed a similar pattern to those for the P2–P1 period with higher degrees of reduction from July to December (Fig. 5a). Variations of both mean monthly and extreme discharges displayed similar patterns to those for the P2–P1 period comparison (Fig. 5c and d). Therefore, successive construction of the cascaded of two dams (i.e., Zhikong and Pangduo) enhanced the changes of the natural flow regime that emerged after the construction of the first dam.

Between periods P2 and P3, the mean monthly discharges increased with moderate and high degrees, while the extreme discharges generally decreased (i.e., the green bars in Fig. 5a and 5b). Their variations mostly followed the patterns of those in the previous two periods of change (i.e., P1–P2 and P1–P3) (Fig. 5c and 5d). These changes indicate that the emergence of the second (Pangduo) dam essentially increased mean monthly discharges except for August and September, particularly for winter low flows, which led to a similar degree of variation for most mean monthly discharges to those in the P1–P3 period.

These patterns among the three periods were further confirmed by their overall degrees of alterations (i.e. D_T), which were 0.421, 0.558, and 0.530 for P1–P2, P1–P3, and P2–P3, respectively. The degree of alteration due to the construction of the first dam was less than that after the completion of the cascade of two dams, which was similar to the degree of alteration cause by the closure of the second dam. Overall, it appeared that both magnitude and variability of the natural flow regime in reaches A and B were reduced with the more increased flow magnitudes during the dry season due to the cumulative effect of the two dams than due to the first dam alone.

3.2.2. Reaches C and D

Changes of the hydrological regime for reaches C and D may be revealed by comparing key hydrological indices between the Tangjia and Lhasa stations. At the Tangjia station, whose data reflect the hydrological regime in reaches A and B, the maximum discharge (Q_{max}, m^3/s) decreased significantly from P1 to P3. In particular, it reduced by 21.5% (Fig. 6a), possibly indicating the cumulative impact of the two dams on hydrological processes. Different from conditions at the Tangjia station, Q_{max} at the Lhasa station marginally decreased from P1 to P2 and even increased slightly from P2 to P3 (Fig. 6a). The lesser degree of Q_{max} reduction during the first two

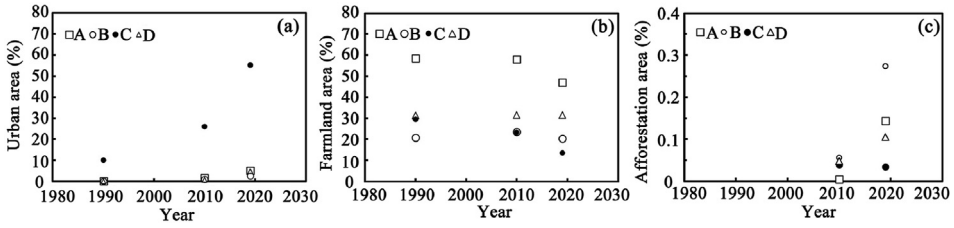

Fig. 4. Historical changes of the four types of human activities from P1 to P3 in the four reaches. (a) Urban area; (b) farmland area; and (c) afforestation area.

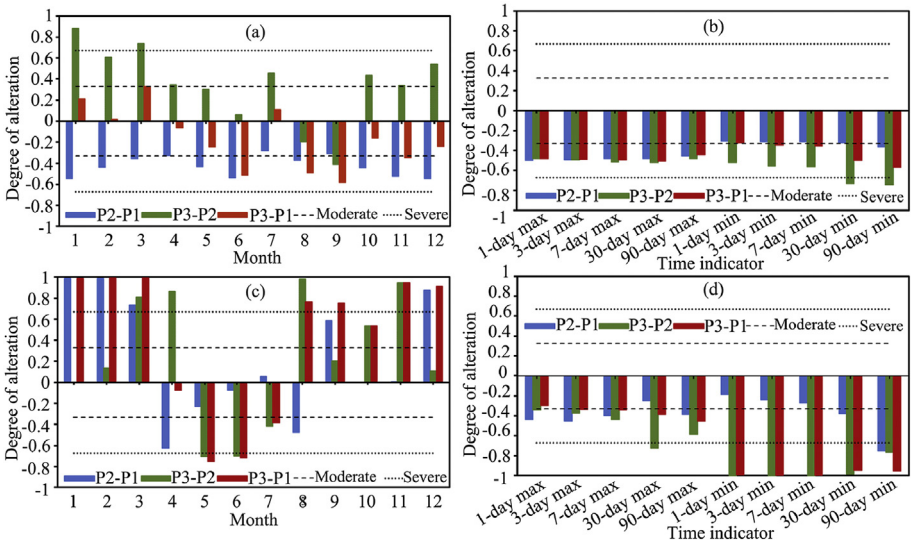

Fig. 5. Results of IHA-RVA. (a) Degree of alteration for the 12 monthly mean discharges; (b) degree of alteration for the 10 minimum and maximum discharges; (c) degree of alteration for the coefficient of variation for the 12 monthly mean discharges; and (d) degree of alteration for the coefficient of variation for the 10 minimum and maximum discharges.

periods reflected the role of the two tributaries to the Lhasa River (Fig. 1a), which compensated for the possible reduction of Q_{max} due to the construction of the first dam. The increase of Q_{max} from P2 to P3 in the Lhasa station further indicated that the impact of the two dams on flows of reaches C and D, which are about 104 km downstream from the Zhikong Dam, diminished during this period.

Over the entire study period (i.e., from P1 to P3), Q_{max} at the Lhasa station was always greater than that at the Tangjia station with the difference increased in P3 (Fig. 6a). This general trend suggests that human activities had limited impact on hydrological extremes in the reaches around the Lhasa station (i.e., reaches C and D). The duration of river flows greater than Q_1 showed different patterns at both stations. Days of channel-forming discharges ($Q > Q_1$) at the Tangjia station decreased from P1 (19.1) to P2 (14.4), because of the construction of the Zhikong (i.e., the first) Dam, but increased from P2 to P3 (18.0) (Fig. 6b). This pattern was consistent with that of the D_T values previously described, suggesting that the second dam (i.e., Pangduo) mainly contributed to reducing the hydrological extremes, but not the duration of high flows. At the Lhasa station, the number of the days slightly increased from P1 to P2 and then decreased marginally from P2 to P3 (Fig. 6b). Again, this pattern indicated that river flows in these reaches (i.e., C and D) were not substantially affected by the cascade of two dams, which may be further illustrated by comparing the mean discharges (Q_m, m^3/s) between the two hydrological stations for the flood period (i.e., from June to September) and the non-flood period (i.e., from October to May) (Fig. 6c).

During P1, the percent changes of Q_m for both periods were similar, which were 17.2% for the non-flood period and 18.6% for the flood period, respectively (Fig. 6c). However, during P2, this percentage for the non-flood period was significantly higher than that for the flood period, suggesting that building the first dam affected the relatively low discharges at a much higher degree than the relatively high flows. During P3, however, this percentage was lower in the non-flood period than that in the flood period and both percentages were lower than those in P1 and P2. This means that completion of the second dam enhanced low flows at the Tangjia station, which led to the decreased percentage of the difference for P3, while it had limited influence on high flows, such that the percentage of the difference was relatively high. In general, the construction of the cascade of two dams discernably changed the hydrological regime for reaches A and B, but had very limited impact on that in reaches C and D.

3.3. Morphological responses to different types of human activities

3.3.1. Channel width and braiding intensity

Among the four reaches, reach A has the lowest W_c and BI_t, in P1, followed by reaches C, B, and D for W_c and C, D, and B for BI_t in an increasing order (Fig. 7a and 7b). This is consistent with the fact that reach A is developed in the narrowest alluvial valley with the mean valley width (W_v) = 2.01 km, which is less than that for reaches B, C, and D (i.e., 3.05, 3.46, and 2.67 km, respectively) (Fig. 1c). These values represent the pre-dam status of the reach morphology that has been affected by very limited human activities (e.g., agriculture and urbanization).

From P1 to P2, W_c in reach A increased, but from P2 to P3, it decreased, leading to an overall decrease from P1 to P3 (Fig. 7a). Nonetheless, the differences in the three pairs of periods were less than 28 m, indicating that their differences were not identifiable from Landsat images. They are not statistically significant either based on two-sample difference tests. Similarly, BI_t remained identical from P1 to P2 and was only reduced by 12.5% from P2 to P3 (Fig. 7b). Given that reach A is the nearest to the downstream dam (i.e., Zhikong) constructed at the beginning of P2, it appears that channel morphology in reach A was not sensitive to the construction of the dam. The insignificantly decreasing tendency of W_c and BI_t from P2 to P3 suggested that the completion of the second dam (i.e., Pangduo) had little impact on channel morphology possibly because it is far away from reach A (Fig. 1a).

In reach B, both W_c and BI_t constantly decreased over the two periods (i.e., from P1 to P2 and from P2 to P3), though the difference of W_c from P2 to P3 was insignificant (i.e., 11.8 m). Because reach B is downstream of reach A, these changes should be more related to other human activities than construction of the cascaded of two dams. Given that the dominant human activities in reach B were afforestation and farming (Table 3 and Fig. 3b), the general decreasing trends of W_c and BI_t were possibly facilitated by stabilized sand/gravel bars as a result of planted trees, which may trap more sediment, and, hence, encourage sediment deposition.

The value of W_c in reach C remained the same from P1 to P2, but increased significantly by 20% from P2 to P3 (Fig. 7a).

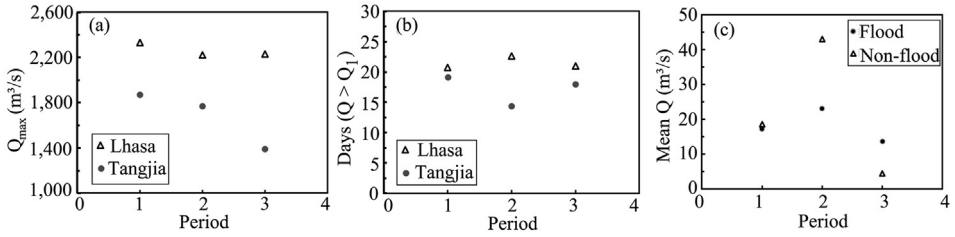

Fig. 6. Comparison of key discharge indices between the Tangjia and Lhasa hydrological stations in the three periods (i.e., P1, P2, and P3). (a) The mean maximum discharges (Q_{max}); (b) the number of days when $Q > Q_1$ where Q_1 is the peak discharge whose return period is one year; and (c) the mean Q for the flood and non-flood periods.

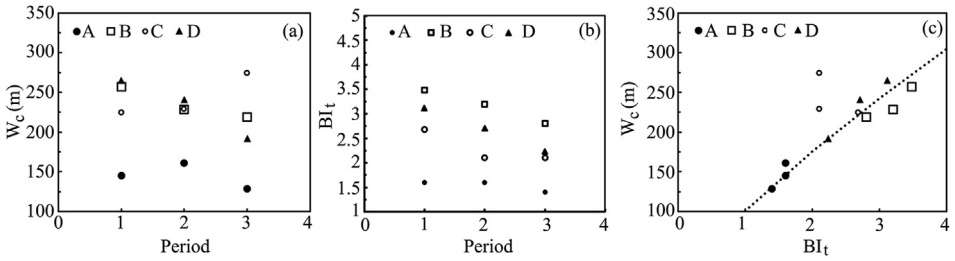

Fig. 7. Temporal patterns of planform morphology for the four reaches. (a) The mean total channel width (W_c); (b) the mean braiding intensity (BI_t); and (c) the relation between W_c and BI_t.

Interestingly, its BI_t value decreased about 22% from P1 to P2 and stayed unchanged from P2 to P3 (Fig. 7b). Since the analyses of hydrological alteration signified that reaches C and D were less affected by the cascaded of two dams, these mixed patterns should be more related to other human activities. Reach C is mostly affected by intensified urbanization and construction including building local check dams for water supply and roads within the valley (Table 3 and Fig. 3c). The increase of the urban area from P1 to P2 was mainly the result of extending the city boundary toward the center of the valley, while from P2 to P3 it was dominated by expanding laterally. This temporal change of the city explained the temporal pattern of BI_t in reach C. The check dams in reach C were constructed in 2013 and 2015–2017. Thus, they were the main human cause for the significant increase of W_c from P2 to P3. The impact of urbanization on reach C was even discernible before the construction of the two dams (i.e., P1), during which BI_t was less than that in reaches B and D, though the three reaches have comparable valley widths (Figs. 1c and 7b). The similar W_c values between P1 and P2 suggests that though the narrowed valley width due to urbanization reduced the braiding intensity, it could have enhanced the flow capacity in the reduced channels, which might lead to channel incision.

Reach D showed that both W_c and BI_t decreased constantly from P1 to P3 (Fig. 7a and 7b). For W_c, the difference between P1 and P2 was within the error of measurement, indicating that the change was undetectable. From P2 to P3, however, the decrease was significant and up to 20%. These morphological changes were more related to human activities other than dam construction because reach D is about 112 km downstream from Zhikong Dam and the hydrological alteration before and after dam completion was very limited (Figs. 5 and 6). The decrease of BI_t should be the consequence of widely distributed farmland on both sides of the braided river system (Fig. 3d), effectively limiting the development of channel branches on the sides. Afforestation on the bars among channel branches, which was mainly implemented after 2010, stabilized bars and possibly caused a lesser degree of BI_t reduction and higher degree of W_c reduction from P2 to P3 than those in the period P1–P2 (Fig. 7a and 7b).

During the period P1 when the braided river system was essentially controlled by natural hydrological processes, W_c and BI_t across all four reaches (i.e., A, B, C, and D) were positively correlated with each other and the correlation was statistically significant (Fig. 7c). This suggests that the studied braided river was a well-connected system under the natural fluvial processes. During the periods P2 and P3, channel morphology has responded to a variety of human activities, such as farming, urbanization, mining, and afforestation (Table 3 and Fig. 4), prompting general reduction of W_c and BI_t (Fig. 7a and 7b). However, this reduction did not seem to affect the connectivity of the braided river system, which is supported by the fact that all points in P2 and P3 still plotted along the curve representing the original W_c–BI_t relation (Fig. 7c) except those for reach C. For a given BI_t value, W_c in P2 and P3 was significantly higher than predicted by the relation, suggesting that the braided river system in reach C was much better connected in these periods than under natural fluvial conditions. This is clearly attributed to the extensive urban sprawling in the valley and ponding of water due to the constructed check dams.

3.3.2. *Lateral shift of the main channel*

The mean annual rate of the lateral shifting of the main channel (R_l) during the period P1–P2 was the lowest in reach A (i.e., 4.32 m/yr), while similar among the other three reaches (i.e., 8.36, 9.22, and 9.55 m/yr for reaches B, C, and D, respectively) (Fig. 8a). This low R_l value in reach A might be attributed to two factors. First, reach A has the narrowest valley width (Fig. 1c), which limited the lateral shift of the channels to a higher degree than that in other reaches under the natural fluvial regime. Second, reach A was affected the most by the reduced magnitude and variability of flows due to the construction of the first dam. It follows that the relatively higher R_l values in reaches B, C, and D should be more related to other types of human activities. However, the coefficient of variation (CV) of R_l was similar in reaches A, B, and C, which was 0.73, 0.78, and 0.72, respectively, larger than that in reach D, which was 0.62. This pattern of variation is hard to interpret at the reach scale.

During the period P2–P3, the R_l value in reach A (11.31 m/yr) was significantly less than that in reach B (24.52 m/yr), but its variation

(i.e., CV = 0.25) was much less than that of the later (i.e., CV = 0.87) (Fig. 8b). Both R_l values were greater than those in the period P1–P2, suggesting that the lateral shift of the main channel during period P2–P3 in these two reaches was more related to other human activities than dam construction as the later reduced the magnitude and frequency of the flows (Figs. 5 and 6), which reduced the probability of channel shifting. Thus, the lesser R_l value in reach A might be affected by the combination of its narrower valley width and higher percentage of the valley area being occupied by human activities (66.5%) including farming, construction, and afforestation (Table 3). The higher variation of the R_l value in reach B reflected that the degree of local channel shifts within the reach greatly varied. The R_l value was 42.47 and 39.41 m/yr in reaches C and D, respectively, with similar variation (i.e., CV = 0.40 and 0.55, respectively). Although the difference was not statistically significant, the higher R_l value in reach C possibly indicates the distinct effect of check dams and intensified urbanization, which narrowed the adjacent river segments, leading to relatively concentrated flow in the immediate upstream and downstream stretches where larger magnitudes of channel shifting were identified (Fig. 3c).

Over the longer period P1–P3, the R_l values in the four reaches (i.e., 3.74, 7.06, 7.76, and 9.21 m/yr, respectively) were very similar to those in period P1–P2 with reduced magnitudes (Fig. 8c). Their variations were less than those in the period P1–P2 for reaches A and D, but similar for reaches B and D (Fig. 8c). The higher R_l values for all reaches in period P2–P3 were related to the shorter period between the two images of P2 and P3, which was only five years, compared to the two images between P1 and P2, which was twenty years. These patterns of R_l values over the three periods with different lengths (Fig. 8a–8c) suggest that (1) R_l values are not comparable between shorter and longer periods and (2) the reduced magnitude and variability of the hydrological regime due to the construction of the two dams do not affect the lateral shift of the main channels at the reach scale.

3.3.3. *Intra-annual changes of the channel width and braiding intensity*

Changes of W_c and BI_t within 2016 reflected the current status of channel morphology in response to a variety of gradually intensified human activities in the study reach. The image in October for reach A was on a different day from that for reach B when its discharge was 144 m^3/s, much less than that for reach B (i.e., 515 m^3/s). Therefore, in a strict sense, values of W_c and BI_t in October are not comparable between reaches A and B, but still useful.

In reaches A and B, the discharge reached the peak in July, and was low before May and after September in 2016 (Fig. 9a). The W_c value was at a maximum in October and it appeared that the maximum W_c in reach B was greater than that in reach A. During the months with low flows, W_c in reach B was always greater than that in reach A. A similar trend existed for the BI_t values for both reaches (Fig. 9b). The generally higher BI_t values in both wet and dry seasons of 2016 in reach B might be more attributable to the possibly higher constraint effect because of the higher percentage of farmland occupation (Table 3). The same effect may explain the wider channels in reach B than those in reach A during the dry season. Therefore, braided channels in reach A are more constrained than those in reach B and more sediment deposition may occur in reach B than in reach A as it has a higher percentage of tree coverage than reach A (Table 3).

In reaches C and D, the discharges also peaked in July and remained low before May and after October (Fig. 9c and 9d). The maximum W_c, which occurred in October, was greater in reach D than that in reach C, but the reverse pattern of lower W_c values prevailed during the dry season with low discharges (Fig. 9c). The maximum BI_t value in reach D was higher than that in reach C, but the lower BI_t values were similar between the two reaches (Fig. 9d). Although farming comprised about 33% of the total area in reach D, much higher than that (about 13%) in reach C, urban areas in reach C occupied about 55% of the total area, much higher than that (about 5%) in reach D (Table 3 and Fig. 4). Thus, reach C is more confined by human activities than reach D, which may explain its lower maximum W_c value. Its higher W_c value during the low flow periods (i.e., the dry season) again reflects the dominant impact of check dams on channel widths. The higher maximum BI_t value in reach D than that in reach C could be ascribed to its relatively higher afforestation coverage (i.e., 10.5%) than reach C (i.e., 3.4%) (Table 3). This impact seems not be very strong, such that during the dry season, the BI_t values in both reaches were similar (Fig. 9d).

3.3.4. *Longitudinal changes of channel width and braiding intensity*

From P1 to P2, the percent change of W_c in the 80 selected transects along the downstream direction did not show any trend in all four reaches (i.e., A, B, C, and D) (Fig. 10a). Similarly, that of N_c demonstrated no-trend with variations around zero (Fig. 10b). The average percent change of W_c in reaches A and B was −14.7% and −1.3%, respectively, while that of N_c was 0 and −13.1%, respectively, suggesting again that the construction of the first dam did not apparently affect W_c values in these two reaches. The maximum percent change of W_c occurred in a transect within reach C where N_c did not change at all (Fig. 10a and 10b). This transect (T50) is located within the extent of Lhasa (Fig. 3c), and, thus, reflects the local response to urbanization. Except for this transect, the variation of the percentage changes of W_c and N_c in reach C was slightly less than that in reach D. This might reflect the relatively high rate of sediment deposition in this reach, as it has more afforestation area than reach D does (Table 3).

From P2 to P3, no downstream trends existed for both W_c and N_c (Fig. 10c and 10d). Reach A experienced no changes for W_c and local changes for N_c, demonstrating no sign of impact from the second dam. The variations in the percent change of both W_c and N_c in reach B were generally higher than those in reach A (Fig. 10a and 10b). These localized higher variations must be related to the spatially variable human activities such as farming and afforestation. Both W_c and N_c within reach C displayed higher degrees of variation in several transects (Fig. 10c and 10d), reflecting the influence of the check dams on channel morphology in reach C. In

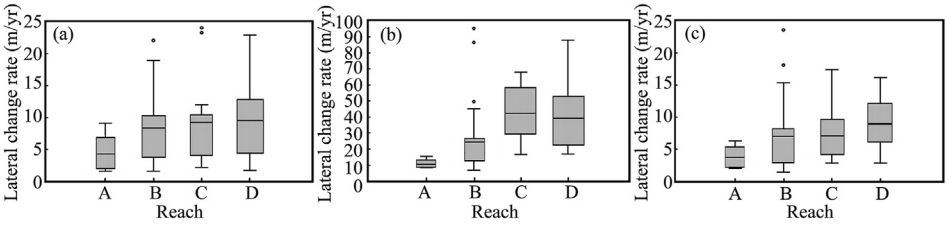

Fig. 8. Rates of the lateral shift of the main channel in the four reaches (the bar inside each box representing the mean value, the top bar referring to the maximum value, the bottom bar referring to the minimum value, and the black point referring to the outlier). (a) The period P1–P2; (b) the period P2–P3; and (c) the period P1–P3.

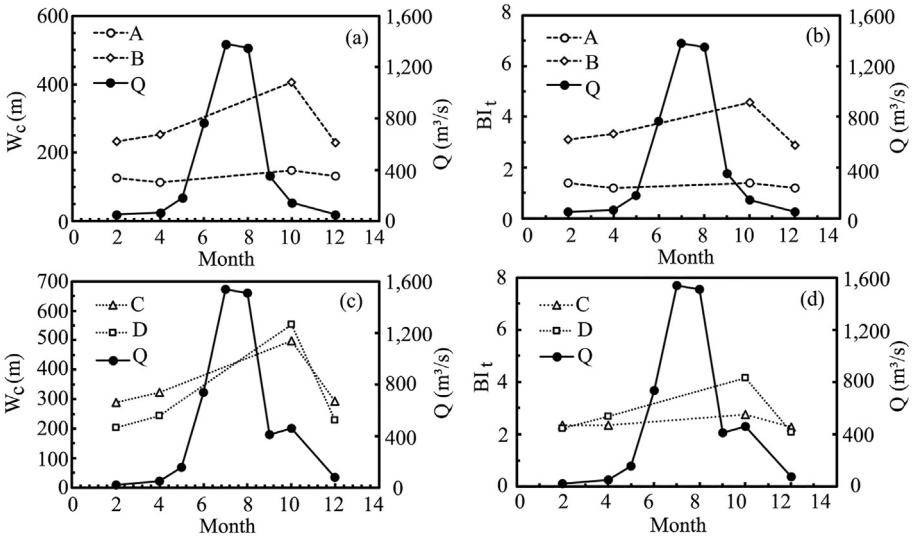

Fig. 9. Intra-annual characteristics of the channel morphology in the four reaches. (a) W_c for reaches A and B; (b) BI_t for reaches A and B; (c) W_c for reaches C and D; and (d) BI_t for reaches C and D.

reach D, the no-trend variations for both W_c and N_c again suggested that the impact of dominant human activities (i.e., farming and afforestation) takes effect at the local spatial scale (i.e., individual transects).

4. Discussion

4.1. Complex impacts of various human activities on channel morphology

Operation of reservoirs created by dams directly affects downstream reaches of the interrupted rivers by altering flow and the flood regime and reducing the amount and size of the flushed sediment (Depret et al., 2019; Jin et al., 2019; Kondolf et al., 2014; Ren et al., 2020). This effect migrates progressively downstream of the impoundment, leading to spatially (how far it might reach) and temporally (how long it may take) variable responses of channel morphology (Arnaud et al., 2015; Ayles & Church, 2014; Downs & Piégay, 2019; Nelson et al., 2013). In the two upstream reaches (i.e., A and B) of the Lhasa River, the magnitude and variability of the natural flow regime after the closure of the first (Zhikong) dam were obviously reduced in terms of the data at the Tangjia station (Figs. 1b and 6). Yet, their further changes due to the completion of the second (Pangduo) dam were limited (Fig. 6), mainly because the dam is located further (65 km) upstream of the study reach.

Interestingly, both the channel width (W_c) and braiding intensity (BI_t) slightly increased from P1 to P2 in reach A (Fig. 7a and 7b), which is the 16-km reach immediately downstream of Zhikong Dam (Fig. 1b). Even in the first four transects that are within 4 km of Zhikong Dam, W_c increased and BI_t remained unchanged from P1 to P2 (Fig. 10a and 10b). Although these patterns are only based on morphological data between two years (i.e., 1990 and 2010), they

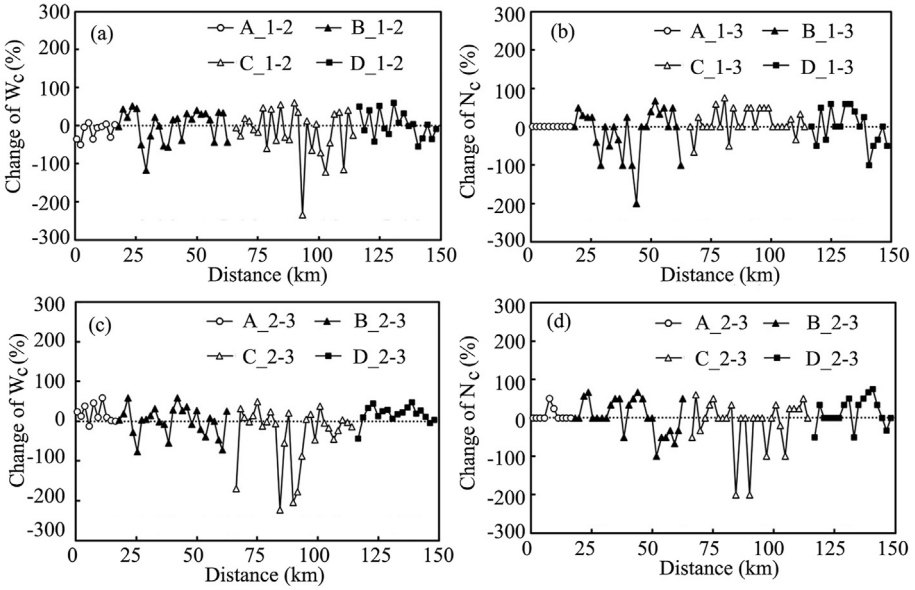

Fig. 10. Longitudinal changes of channel planform morphology in the four reaches. (a) Changes of W_c for period P1–P2; (b) changes of BI_t for period P1–P2; (c) changes of W_c for period P2–P3; and (d) changes of BI_t for period P2–P3.

are statistically significant and apparently at odds with many studies showing channel narrowing and reduced braiding after dam construction due to bed degradation (Chen et al., 2019; Gordon & Meentemeyer, 2006; Petts & Gurnell, 2005; Piégay et al., 2009; Surian & Rinaldi, 2003).

A frequently associated consequence of bed degradation is coarsening of grains on the bed surface due to the armoring effect (Grant, 2012). The current grain size analysis performed in 2018 based on a method similar to the Wolman pebble count method (Wolman, 1954) showed that surface grains in reach A are significantly coarser than those in the three downstream reaches (Fig. 11). While the mean slope of reach A is about 24% greater than that of reach B, the median grain (i.e., D50) in the former is more than 200% coarser than that in the latter. This suggests that the coarsening must be mainly (if not completely) contributed from the dam impact rather than from the natural downstream fining process commonly seen in gravel-bed rivers. If the coarsening is induced by the so-called "starved water", which refers to supply-limited flows due to the fact that dams tend to reduce sediment load more than water discharge in the downstream reaches (Pique et al., 2017), then one should expect narrowed channel widths and reduced complexity of braiding (Stecca et al., 2019).

This generally unchanged channel morphology with a coarsened bed surface from P1 to P2 suggests that the channel morphology of reach A might have already recovered from its quick reaction to alteration of the hydrological regime and sediment movement four years after the (Zhikong) dam construction, as Zhikong Dam was built in 2006, while the Landsat image representing channel morphology in P2 was obtained in 2010. In other words, the studied braided reach of the Lhasa River likely may have a very short relaxation period (Graf, 1977), compared with many dam-impacted downstream rivers (Greenwood et al., 1999; Petts & Greenwood, 1985; Sanchis-Ibor et al., 2019; Vericat et al., 2008). Although the lack of a detailed historical series of data may undermine this assertion, it is argued that the assertion can be supported by evidence from three different aspects. The first is related to climate conditions. The Lhasa River is dominated by a semi-arid climate that is evidenced by (1) low annual precipitation and high annual evaporation and (2) the fact that the study reaches have been subject to aeolian processes capable of mobilizing sand on bars and the braidplain (Chang, 2007). Many studies have demonstrated that river systems under semi-arid and/or Mediterranean climates are very sensitive to external forces (e.g., dam interruption), and readily change to a new quasi-equilibrium status, leading to a short relaxation time (Petts & Gurnell, 2005). The second aspect considers the morphodynamic features of reach A. Because this reach is located immediately downstream of Zhikong Dam, its transport capacity should be reduced the most compared with that in other three reaches (Brenna et al., 2020; Wright & Minear, 2019). In addition, reach A as a gravel bed. Such a riverbed should experience less pronounced channel incision due to dam construction as pointed out by Grant (2012), which may be further supported by the fact that Zhikong Dam reduced both the magnitude of peak discharges and their duration (Fig. 7a and 7b). Therefore, the altered flow regime likely coarsened the bed surface by transporting fine and medium-sized grains out of the reach, while causing limited changes of channel widths and braiding intensity, which allowed reach A to recover and quickly reach a new equilibrium condition. The third aspect is related to the hydrological nature of the studied river reach. The maximum volume of water that can be stored storage by the two dams only comprises about 10% of the total annual runoff passing through reach A. This means that the degree of hydrological alteration caused by the two dams is relatively small, and, thus, the induced morphological changes are limited and the morphology can more easily recover.

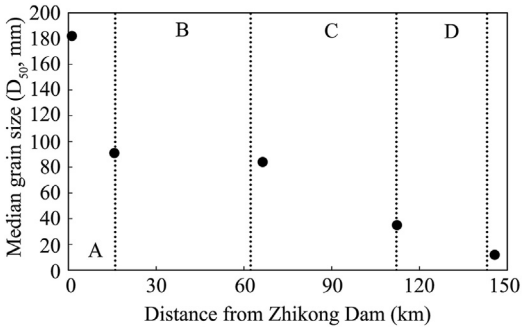

Fig. 11. Longitudinal trend of the median sizes of bed-surface grains over the four study reaches (i.e., A, B, C, and D).

The construction of the second (i.e., Pangduo) dam further reduced the magnitude of the maximum discharges, but increased the frequency of the medium high flows (Fig. 6a–6c), which would encourage vegetation encroachment. Also, not only a proportion of farmland (about 10%) but also many bars between braided channels were occupied by planted trees (Fig. 4b and 4c). The increased vegetation coverage from P2 to P3 might have played a dominant role in the decreasing W_c and BI_t during this period in reach A (Fig. 7a and 7b). In as much as reach B is 16 km downstream of reach A (Fig. 1b), the continuous decrease of W_c and BI_t from P1 to P2 and P3 could be more responsive to increased farming and afforestation (accounting for 20.4% and 27.3% of the valley area, respectively), because morphological response to damming is more sensitive in the immediate downstream reach (e.g., about 5 km) (Brenna et al., 2020; Surian & Rinaldi, 2003).

4.2. Morphological trajectories under different types of human activities

The four smaller reaches in the study reach of the Lhasa River have different physiographic settings and dominant types of human activities (Fig. 1c and Table 3). From reach A to reach C, the mean valley slope (S_v) decreases while the mean valley width (W_v) increases (Fig. 1c), indicating that the valley gradually becomes broader and gentler in the downstream direction. However, in reach D, S_v suddenly increases to the highest value among the four (i.e., 0.77%) with decreased W_v. From reach A to reach D, the dominant type of human disturbance is farming (higher degree), afforestation/farming, urban areas, and farming (lower degree), respectively (Table 3). From 1990 to 2019, urban areas in all reaches have generally increased with the highest increase rate in reach C, whereas farmland decreased drastically in reaches A and C, but remained almost similar in the other two reaches (Fig. 4a and 4b). Therefore, the historical evolution of human interference with the river channels is different in these four reaches with variable physiographic characteristics.

Over the entire study period (i.e., 1990–2019), the increase of the urban area has caused a consistent decrease of W_c in reaches B and D, and a parallel trend with a lesser magnitude in reach A, regardless of their different physical settings (Fig. 12a). However, in reach C, W_c increased with the urban area (Fig. 12a). This opposite trend is mainly due to the construction of the check dams (see site 2 in Fig. 3c), which is obviously for satisfying the increasing demand for water usage from Lhasa with continuously increased population. Interestingly, for BI_t, reach C followed the trend of reach B, and reach D and A retained a similar trend (Fig. 12b). These trends suggest that channel planform morphology

(i.e., W_c and BI_t) responds to the expansion of the urban area in a similar style – that is, reducing the complexity of the braiding system.

As the farmland increases, W_c in all reaches decreased consistently with a greater rate than that for the urban area (Fig. 12a and 12c). BI_t followed a similar trend for all reaches except one point representing the current farmland in reach C (Fig. 12d), again reflecting the significant effect of backwater created by the check dams. These consistent trends over all four reaches further suggest that trajectories of morphological changes in these braided river reaches due to farming are similar. The impact of afforestation on channel morphology is largely stabilizing bars at local scales (Bertoldi et al., 2011; Maeno & Watanabe, 2008). By comparing the number of channels (N_c) between vegetated and non-vegetated transects in P3, it was found that N_c in vegetated transects is generally larger than that in the non-vegetated transects. Yet, this pattern does not affect BI_t values at the reach scale.

Since the impact of urban areas and farming on river morphology is not mutually independent in reality and the increase in the urban area typically causes the decrease of farmland in the studied reaches of the Lhasa River valley, the identified morphological responses are the lumped effect of both types of human activities (Fig. 7a and 7b). Thus far, 47%–66% of the four reaches have been disturbed by construction (mainly urbanization), farming, and afforestation (Table 3). There is limited space to accommodate new urban area and farmlands. Therefore, future development of these human activities must lead to more farmland being replaced by urban usage, which will further force the braided river to gradually transform toward a single-thread wandering river (Fig. 12b and 12c). This is a common trend that has been observed in many other disturbed braided rivers (Llena et al., 2020; Stecca et al., 2019; Surian & Rinaldi, 2003). Since 1990, the expansion of Lhasa has narrowed the impacted section of reach C by up to 70% (i.e., T47 and T53 in Fig. 3). In the meantime, more days with $Q > Q_5$ occurred after the completion of the Zhikong Dam (i.e., 2005) than during the period before. There were only 7 days in the 1990–2005 period, while 11 days after 2005 with 4 days in 2014. This trend of increasing extreme discharges is expected to continue under the influence of climate change (Allan & Soden, 2008; Apurv et al., 2015). Therefore, Lhasa will face a higher possibility of flooding in the future. The current analyses suggest that adjusting the flow regime by operating the cascaded of two dams will not be sufficient because flows in reaches C and D where Lhasa is and will be extended to are also supplied from the three tributaries (Fig. 1b). Therefore, new management strategies are required to regulate flows in these tributaries for avoiding potential future flooding in Lhasa, in addition to the existing management practices.

5. Conclusions

The Lhasa River is a heavily disturbed braided river on the Qinghai-Tibet Plateau. It is disturbed by a variety of human activities mainly including dam building, urbanization, agricultural development, afforestation, and gravel mining. Assessment of the impact of these disturbances on river morphology begins a journey of understanding how fluvial systems in this physically unique region, with very high elevations and diverse climate conditions, have responded to gradually intensified anthropogenic activities and predicting the directions, toward which rivers in this region will evolve. The available hydrological data allowed that the alternating of the natural hydrological regime in reaches A and B because of the construction of a cascade of two dams, the first (Zhikong) one immediately upstream of the studied reach, to be shown. The alteration is reflected by the reduction of both magnitude and variability of river flows. However, for the two further downstream reaches (i.e., C and D), the dam-induced hydrological alteration is diminished because (i) their locations are further downstream from the dams; and (ii) three tributaries contribute additional natural flows to these reaches.

Although the limited number of remote sensing images selected in the current study prevented evaluation of the full spectrum of historical changes of the channel morphology, the error evaluation assured that comparisons of the extracted channel morphology from these images are meaningful. In reach A, which is supposed to be most sensitive to the dam construction, the altered flow regime did not lead to a narrowed channel width and reduced braiding

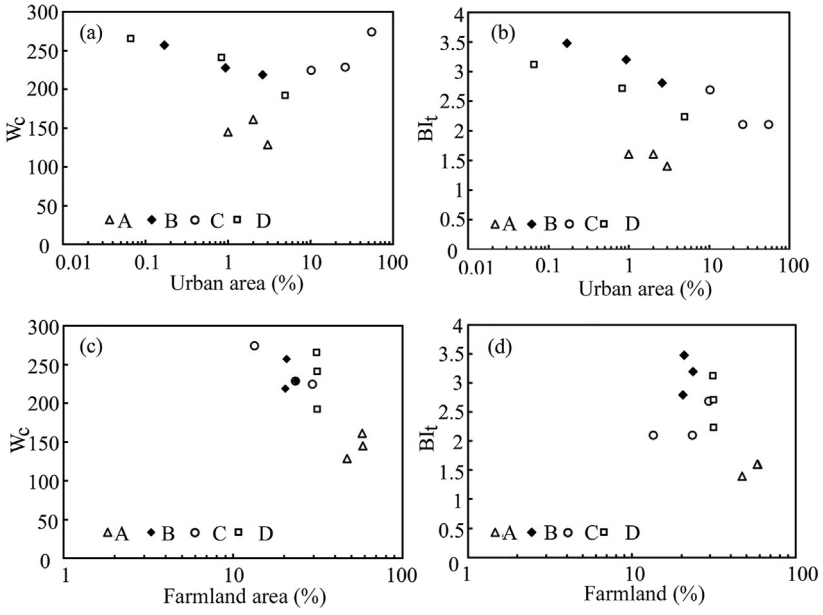

Fig. 12. Relation between historically variable human activities and the channel planform response in the four reaches. (a) W_c vs. urban area; (b) BI_t vs. urban area; (c) W_c vs. farmland area; and (d) BI_t vs. farmland area.

intensity, as found in many braided rivers located in other regions of the world. This discrepancy is attributed to the possibility that the downstream reach of the Lhasa River has a short relaxation time due to its semi-arid climate, reduced transport capacity, and limited impact of altered hydrology on channel morphology. These natural features highlight the variable roles of different dams and reservoirs in interrupting the downstream reaches and the importance of acquiring site-specific information for future river management (Csiki & Rhoads, 2014).

The complex impact of human activities on the studied reach of the Lhasa River is embodied in not only multiple types of activities, but also their spatial and temporal variations. At the reach scale, channel morphology has generally changed toward a simpler structure by reducing both W_c and BI_t from P1 to P3, reflecting the increasing constraints on river evolution due to increased occupation of the valley area by urbanization and farming. Afforestation has increased vegetation coverage on bars, and, thus, has enhanced their stability. However, its impact on channel morphology tends to still be felt at the local scale (i.e., individual cross sections). Mining did not appear to affect channel morphology significantly, probably because its extent is very limited. Over the entire study period (i.e., from 1985 to 2019), different types of human activities have developed at different rates in different reaches (i.e., A, B, C, and D). However, the response of river morphology (i.e., W_c and BI_t) to these dynamic activities has followed similar trajectories except in reach C where water ponding by check dams drastically increased the channel width. This pattern confirms the recent finding that river reaches with variable physiographic contexts often follow similar trajectories in responding the impact of dynamic human activities on their morphology (Stecca et al., 2019).

While growing research has focused on morphological and ecological responses to dam removal (Tullos et al., 2014; Warrick et al., 2015), rivers originating from the Qinghai-Tibet Plateau including those flowing through China, India, Nepal, and Pakistan have been experiencing a surge of dam construction because they generally have steep channel gradients and relatively narrow valleys. This study provides a process-based perspective for assessing the impact of human activities on the braided Lhasa River and may be used in the future for scientific assessment of environmental protection and ecological risk of other dams in the region.

Declaration of competing interest

The authors declare that they have no known competing financial interests or personal relationships that could have appeared to influence the work reported in this paper.

Acknowledgements

This study was supported by the National Natural Science Foundation of China (Grant Nos. 91647204, 51979012, and 51809086), Fundamental Research Funds for the Central Universities (No. 2042021kf0199), Natural Science Foundation of Hunan Province of China (Grant No. 2020JJ3036), and Research Foundation of the Education Department of Hunan Province of China (Grant No. 19A017). The authors thank the two anonymous reviewers and the editor for insightful comments and suggestions that improved the quality and English language of the original manuscript.

References

Allan, R. P., & Soden, B. J. (2008). Atmospheric warming and the amplification of precipitation extremes. *Science, 321*(5895), 1481–1484.

Apurv, T., Mehrotra, R., Sharma, A., Goyal, M. K., & Dutta, S. (2015). Impact of climate change on floods in the Brahmaputra basin using CMIP5 decadal predictions. *Journal of Hydrology, 527*, 281–291.

Arnaud, F., Piegay, H., Schmitt, L., Rollet, A. J., Ferrier, V., & Beal, D. (2015). Historical geomorphic analysis (1932-2011) of a by-passed river reach in process-based restoration perspectives: The Old Rhine downstream of the Kembs diversion dam (France, Germany). *Geomorphology, 236*, 163–177.

Ashmore, P. (2013). Morphology and dynamics of braided rivers. In J. Shroder (Ed.), *Treatise on geomorphology* (pp. 289–312). San Diego, CA: Academic Press.

Ashmore, P., Bertoldi, W., & Gardner, J. T. (2011). Active width of gravel-bed braided rivers. *Earth Surface Processes and Landform, 36*, 1510–1521.

Ayles, C. P., & Church, M. (2014). Downstream channel gradation in the regulated Peace River. In M. Church (Ed.), *The regulation of peace river: A case study for river management* (pp. 39–66). Chichester, UK: John Wiley & Sons.

Bakker, M., Antoniazza, G., Odermatt, E., & Lane, S. N. (2019). Morphological response of an alpine braided reach to sediment-laden flow events. *Journal of Geophysical Research: Earth Surface, 124*, 1310–1328.

Belletti, B., Dufour, S., & Piégay, H. (2012). Regional variability of aquatic pattern in braided reaches (example of the French Rhône basin). *Hydrobiology, 712*, 25–41.

Bertoldi, W., Drake, N. A., & Gurnell, A. M. (2011). Interactions between river flows and colonizing vegetation on a braided river: Exploring spatial and temporal dynamics in riparian vegetation cover using satellite data. *Earth Surface Processes and Landforms, 36*(11), 1474–1486.

Bertoldi, W., Gurnell, A., Surian, N., Tockner, K., Zanoni, L., Ziliani, L., & Zolezzi, G. (2009). Understanding reference processes: Linkages between river flows, sediment dynamics and vegetated landforms along the Tagliamento River, Italy. *River Research and Applications, 25*, 501–516.

Bertoldi, W., Zanoni, L., & Tubino, M. (2009). Planform dynamics of braided streams. *Earth Surface Processes and Landforms, 34*, 547–557.

Boruah, S., Gilvear, D., Hunter, P., & Sharma, N. (2008). Quantifying channel planform and physical habitat dynamics on a large braided river using satellite data—the Brahmaputra, India. *River Research and Applications, 24*, 650–660.

Brenna, A., Surian, N., & Mao, L. (2020). Response of a gravel-bed river to dam closure: Insights from sediment transport processes and channel morphodynamics. *Earth Surface Processes and Landforms, 45*(3), 756–770.

Chalise, D. R., Sankarasubramanian, A., & Ruhi, A. (2021). Dams and climate interact to alter river flow regimes across the United States. *Earth's Future, 9*, e2020EF001816.

Chang, C. P. (2007). A study on comprehensive renovation of sand source in the valley of lower reaches of Lhasa River, Tibet Plateau. *Reseach of Soil Water Conservation, 14*, 219–222. (*In Chinese*)

Chen, F., Chen, L., Zhang, W., Han, J. D., & Wang, J. Z. (2019). Responses of channel morphology to flow-sediment variations after dam construction: A case study of the Shashi reach, middle Yangtze river. *Hydrology Research, 50*(5), 1359–1375.

Chien, N. (1985). Changes in river regime after the construction of upstream reservoirs. *Earth Surface Processes and Landforms, 10*, 143–159.

Csiki, S. J. C., & Rhoads, B. L. (2014). Influence of four run-of-river dams on channel morphology and sediment characteristics in Illinois, USA. *Geomorphology, 206*, 215–229.

Depret, T., Piégay, H., Dugue, V., Vaudor, L., Faure, J. B., Le Coz, J., & Camenen, B. (2019). Estimating and restoring bedload transport through a run-of-river reservoir. *Science of the Total Environment, 654*, 1146–1157.

Downs, P. W., & Piégay, H. (2019). Catchment-scale cumulative impact of human activities on river channels in the late Anthropocene: Implications, limitations, prospect. *Geomorphology, 338*, 88–104.

Dubey, A. K., Gupta, P., Dutta, S., & Kumar, B. (2014). Evaluation of satellite-altimetry-derived river stage variation for the braided Brahmaputra River. *Internatinoal Journal of Remote Sensing, 35*, 7815–7827.

Gao, Y. X., Vogel, R. M., Kroll, C. N., Poff, N. L., & Olden, J. D. (2009). Development of representative indicators of hydrologic alteration. *Journal of Hydrology, 374*(1–2), 136–147.

Gao, B., Yang, D. W., Zhao, T. T. G., & Yang, H. B. (2012). Changes in the eco-flow metrics of the upper Yangtze river from 1961 to 2008. *Journal of Hydrology, 448*, 30–38.

Gierszewski, P. J., Habel, M., Szmanda, J., & Luc, M. (2020). Evaluating effects of dam operation on flow regimes and riverbed adaptation to those changes. *Science of the Total Environment, 710*, 136202.

Gordon, E., & Meentemeyer, R. K. (2006). Effects of dam operation and land use on stream channel morphology and riparian vegetation. *Geomorphology, 82*(3–4), 412–429.

Graf, W. L. (1977). The rate law in fluvial geomorphology. *American Journal of Science, 272*, 178–191.

Grant, G. E. (2012). The geomorphic response of gravel-bed rivers to dams: Perspectives and prospects. In M. Church, P. M. Biron, & A. G. Roy (Eds.), *Gravel-bed rivers: Processes, tools, environments* (pp. 165–181). Hoboken, NJ: Wiley.

Gran, K. B., Tal, M., & Wartman, E. D. (2015). Co-evolution of riparian vegetation and channel dynamics in an aggrading braided river system, Mount Pinatubo, Philippines. *Earth Surface Processes and Landforms, 40*, 1101–1115.

Greenwood, M. T., Bickerton, M. A., Gurnell, A. M., & Petts, G. E. (1999). Channel changes and invertebrate faunas below Nant-y-Moch dam, river Rheidol, Wales, UK: 35 Years on. *Regulated Rivers-Research & Management, 15*(1–3), 99–112.

Han, M. Q., Brierley, G., Li, B., Li, Z. W., & Li, X. L. (2020). Impacts of flow regulation on geomorphic adjustment and riparian vegetation succession along an anabranching reach of the Upper Yellow River. *Catena, 190*, 104561.

Jiang, C., Zhang, Q., & Luo, M. M. (2019). Assessing the effects of the Three Gorges Dam and upstream inflow change on the downstream flow regime during different operation periods of the dam. *Hydrological Processes, 33*(22), 2885–2897.

Jin, W. T., Chang, J. X., Wang, Y. M., & Bai, T. (2019). Long-term water-sediment multi-objectives regulation of cascade reservoirs: A case study in the upper Yellow River, China. *Journal of Hydrology, 577*, 123978.
Ju, J. C., & Masek, J. G. (2016). The vegetation greenness trend in Canada and US Alaska from 1984-2012 Landsat data. *Remote Sensing of Environment, 176*, 1–16.
Kondolf, G. M., Gao, Y. X., Annandale, G. W., Morris, G. L., Jiang, E. H., Zhang, J. H., Cao, Y. T., Carling, P., Fu, K. D., Guo, Q. C., Hotchkiss, R., Peteuil, C., Sumi, T., Wang, H. W., Wang, Z. M., Wei, Z. L., Wu, B. S., & Yang, C. T. (2014). Sustainable sediment management in reservoirs and regulated rivers: Experiences from five continents. *Earth's Future, 2*(5), 256–280.
Ligon, F. K., Dietrich, W. E., & Trush, W. J. (1995). Downstream ecological effects of dams. *BioScience, 45*, 183–192.
Li, D. F., Li, Z. W., Zhou, Y. J., & Lu, X. X. (2020a). Substantial increase in the water and sediment fluxes in the headwater region of the Tibetan Plateau in response to global warming. *Geophysical Research Letters, 47*, e2020GL087745.
Li, D. N., Long, D., Zhao, J. S., Lu, H., & Hong, Y. (2017). Observed changes in flow regimes in the Mekong River basin. *Journal of Hydrology, 551*, 217–232.
Li, Z. W., Lu, H. Y., Gao, P., You, Y. C., & Hu, X. Y. (2020b). Characterizing braided rivers in two nested watersheds in the source region of the Yangtze river on the Qinghai-Tibet Plateau. *Geomorphology, 351*, 106945.
Limaye, A. B. (2017). Extraction of multithread channel networks with a reduced-complexity flow model. *Journal of Geophysical Research: Earth Surface, 122*, 1972–1990.
Li, J., Xia, J., Zhou, M., Deng, S., & Wang, Z. (2018). Channel geometry adjustments in response to hyperconcentrated floods in a braided reach of the Lower Yellow River. *Progress in Physical Geography-Earth and Environemnt, 42*(3), 352–368.
Li, X. J., & Xu, L. Y. (2015). Feature of riparian soil elements induced by hydropower development in Lhasa River. *Environmental Science and Technology, 38*, 148–156. (*In Chinese*)
Li, Z. W., Yu, G. A., Brierley, G., & Wang, Z. Y. (2016). Vegetative impacts upon bedload transport capacity and channel stability for differing alluvial planforms in the Yellow River Source Zone. *Hydrology and Earth System Sciences, 20*, 3013–3025.
Llena, M., Vericat, D., Martinez-Casasnovas, J. A., & Smith, M. W. (2020). Geomorphic adjustments to multi-scale disturbances in a mountain river: A century of observations. *Catena, 192*, 104548.
Lotsari, E., Wainwright, D., Corner, G. D., Alho, P., & Käyhkö, J. (2014). Surveyed and modelled one-year morphodynamics in the braided lower Tana River. *Hydrological Processes, 28*, 2685–2716.
Maeno, S., & Watanabe, S. (2008). Field experiment to restore a gravel bar and control growth of trees in the Asahi River. *International Journal of River Basin Management, 6*(3), 225–232.
Magilligan, F. J., & Nislow, K. H. (2005). Changes in hydrologic regime by dams. *Geomorphology, 71*(1–2), 61–78.
Ma, Z. Z., Wang, Z. J., Xia, T., Gippel, C. J., & Speed, R. (2014). Hydrograph-based hydrologic alteration assessment and its application to the Yellow River. *Journal of Environmental Informatics, 23*(1), 1–13.
Nelson, N. C., Erwin, S. O., & Schmidt, J. C. (2013). Spatial and temporal patterns in channel change on the Snake River downstream from Jackson Lake dam, Wyoming. *Geomorphology, 200*, 132–142.
Nilsson, C., Jansson, R., & Zinko, U. (1997). Long-term responses of river-margin vegetation to water-level regulation. *Science, 276*, 798–800.
Ozyavuz, M., Bilgili, B. C., & Salici, A. (2015). Determination of vegetation changes with NDVI method. *Journal of Environmental Protection and Ecology, 16*(1), 264–273.
Paetzold, A., Schubert, C. J., & Tockner, K. (2005). Aquatic terrestrial linkages along a braided-river: Riparian arthropods feeding on aquatic insects. *Ecosystems, 8*, 748–759.
Petts, G. E., & Greenwood, M. (1985). Channel changes and invertebrate faunas below Nant-Moch dam, river Rheidol, Wales, UK. *Hydrobiologia, 122*(1), 65–80.
Petts, G. E., & Gurnell, A. M. (2005). Dams and geomorphology: Research progress and future directions. *Geomorphology, 71*(1–2), 27–47.
Piégay, H., Grant, G., Nakamura, F., & Trustrum, N. (2009). Braided river management: From assessment of river behaviour to improved sustainable development. In I. Jarvis, G. H. Sambrook Smith, J. L. Best, C. S. Bristow, & G. E. Petts (Eds.), *Braided rivers: Process, deposits, ecology and management* (pp. 257–275). Oxford, UK: Blackwell.
Pique, G., Batalla, R. J., Lopez, R., & Sabater, S. (2017). The fluvial sediment budget of a dammed river (upper Muga, southern Pyrenees). *Geomorphology, 293*, 211–226.
Poff, N. L., Allan, J. D., Bain, M. B., Karr, J. R., Prestegaard, K. L., Richter, B. D., Sparks, R. E., & Stromberg, J. C. (1997). The nature flow regime. *BioScience, 47*(11), 769–784.
Remo, J. W. F., Ickes, B. S., Ryherd, J. K., Guida, R. J., & Therrell, M. D. (2018). Assessing the impacts of dams and levees on the hydrologic record of the Middle and Lower Mississippi River, USA. *Geomorphology, 313*, 88–100.
Ren, J. Q., Zhao, M. D., Zhang, W., Xu, Q. X., Yuan, J., & Dong, B. J. (2020). Impact of the construction of cascade reservoirs on suspended sediment peak transport variation during flood events in the Three Gorges Reservoir. *Catena, 188*, 104409.
Richard, G. A., Julien, P. Y., & Baird, D. C. (2005). Case study: Modeling the lateral mobility of the Rio Grande below Cochiti dam, New Mexico. *Journal of Hydraulic Engineering, 131*, 931–941.
Richter, B. D., Baumgartner, J. V., Braun, D. P., & Powell, J. (1998). A spatial assessment of hydrologic alteration within a river network. *Regulated Rivers-Research and Management, 14*(4), 329–340.
Richter, B. D., Baumgartner, J. V., Powell, J., & Braun, D. P. (1996). A method for assessing hydrologic alteration within ecosystems. *Conservation Biology, 10*(4), 1163–1174.
Sanchis-Ibor, C., Segura-Beltran, F., & Navarro-Gomez, A. (2019). Channel forms and vegetation adjustment to damming in a Mediterranean gravel-bed river (Serpis River, Spain). *River Research and Applications, 35*(1), 37–47.
Schuurman, F., Marra, W. A., & Kleinhans, M. G. (2013). Physics-based modeling of large braided sand-bed rivers: Bar pattern formation, dynamics, and sensitivity. *Journal of Geophysical Research: Earth Surface, 118*, 2509–2527.
Shields, F. D., Jr., & Milhous, R. T. (1992). Sediment and aquatic habitat in river systems. *Journal of Hydraulic Engineering, 118*, 669–687.
Sojka, M., Jaskula, J., Wicher-Dysarz, J., & Dysarz, T. (2016). The impact of the Kowalskie Reservoir on the hydrological regime alteration of the Glowna River. *Journal of Ecological Engineering, 17*(4), 91–98.
Song, X. X., Zhuang, Y. H., Wang, X. L., Li, E. H., Zhang, Y. Y., Lu, X. R., Yang, J., & Liu, X. (2020). Analysis of hydrologic regime changes caused by dams in China. *Journal of Hydrologic Engineering, 25*(4), 05020003.
Stecca, G., Zolezzi, G., Hicks, D. M., & Surian, N. (2019). Reduced braiding of rivers in human-modified landscapes: Converging trajectories and diversity of causes. *Earth-Science Reviews, 188*, 291–311.
Surian, N., & Rinaldi, M. (2003). Morphological response to river engineering and management in alluvial channels in Italy. *Geomorphology, 50*(4), 307–326.
Tao, K., Liu, Y. X., Ke, T., Zhang, Y. R., Xiao, L., Li, S. X., Wei, S. J., Chen, L. Z., & Hu, T. S. (2019). Patterns of bacterial and archaeal communities in sediments in response to dam construction and sewage discharge in Lhasa River. *Ecotoxicology and Environmental Safety, 178*, 195–201.
Tullos, D. D., Finn, D. S., & Walter, C. (2014). Geomorphic and ecological disturbance and recovery from two small dams and their removal. *PloS One, 9*(9), e108091.
Vericat, D., Batalla, R. J., & Garcia, C. (2008). Bed-material mobility in a large river below dams. *Geodinamica Acta, 21*, 3–10.
Wang, Z. Y., Li, Z. W., Xu, M. Z., & Yu, G. A. (Eds.). (2016). *River morphodynamics and stream ecology of the Qinghai-Tibet Plateau*. The Netherland: CRC Press, Taylor & Francis Ltd.
Wang, Z. Y., Wu, B. S., & Wang, G. Q. (2007). Fluvial processes and morphological response in the yellow and Weihe rivers to closure and operation of Sanmenxia dam. *Geomorphology, 91*, 65–79.
Warrick, J. A., Bountry, J. A., East, A. E., Magirl, C. S., Randle, T. J., Gelfenbaum, G. R., Ritchie, A. C., Pess, G. R., Leung, V., & Duda, J. J. (2015). Large-scale dam removal on the Elwha River, Washington, USA: Source-to-sink sediment budget and synthesis. *Geomorphology, 246*, 729–750.
Wolman, M. G. (1954). A method of sampling coarse river-bed material. *Transaction American Geophysical Union, 35*(6), 951–956.
Wright, S. A., & Minear, J. T. (2019). Dam effects on bedload transport on the upper Santa Ana River, California, and implications for native fish habitat. *River Research and Applications, 35*(6), 632–645.
Wu, X., Li, Z., Gao, P., Huang, C., & Hu, T. (2018). Response of the downstream braided channel to Zhikong reservoir on Lhasa River. *Water, 10*, 1144.
Xia, J. Q., Li, X. J., Li, T., Zhang, X., & Zong, Q. (2014). Response of reach-scale bankfull channel geometry in the Lower Yellow River to the altered flow and sediment regime. *Geomorphology, 213*, 255–265.
Xu, H. Q. (2006). Modification of normalised difference water index (NDWI) to enhance open water features in remotely sensed imagery. *International Journal of Remote Sensing, 27*(14), 3025–3033.
Yang, H. J., & Hu, L. J. (2013). Reconciling the regulations and conservation of the Lhasa River, Tibet. *Journal of Soil and Water Conservation, 68*, 55–57. (*In Chinese*)
Yu, C. X., Yin, X. A., & Yang, Z. F. (2016). A revised range of variability approach for the comprehensive assessment of the alteration of flow regime. *Ecological Engineering, 96*, 200–207.
Zhang, Y. L., Wang, C. L., Bai, W. Q., Wang, Z. F., Tu, Y. L., & Yangjaen, D. G. (2010). Alpine wetlands in the Lhasa River basin, China. *Journal of Geographical Sciences, 20*, 375–388.
Zhang, Y., Wang, G. X., & Wang, Y. B. (2011). Changes in alpine wetland ecosystems of the Qinghai-Tibetan plateau from 1967-2004. *Environmental Monitoring and Assessment, 180*, 189–199.
Zhou, W., Li, Z., Ji, S., Hua, C., & Fan, W. (2015). A new index model NDVI-MNDWI for water object extraction in hybrid area. In F. Bian, & Y. Xie (Eds.), *Geo-informatics in resource management and sustainable ecosystem. Communications in Computer and Information Science* (Vol. 482, pp. 513–519). Berlin-Heidenberg: Springer.
Ziliani, L., Surain, N., Botter, G., & Mao, L. (2020). Assessment of the geomorphic effectiveness of controlled floods in a braided river using a reduced-complexity numerical model. *Hyrology and Earth System Sciences, 24*, 3229–3250.
Ziliani, L., & Surian, N. (2012). Evolutionary trajectory of channel morphology and controlling factors in a large gravel-bed river. *Geomorphology, 173*, 104–117.